

*submitted to The Astrophysical Journal Letters on June 25, 1998*

## Circumnuclear Keplerian Disks in Galaxies<sup>1</sup>

Francesco Bertola<sup>2</sup>, Michele Cappellari<sup>2</sup>, José G. Funes, S.J.<sup>2</sup>, Enrico M. Corsini<sup>3</sup>, Alessandro Pizzella<sup>4</sup> & Juan C. Vega Beltrán<sup>5</sup>

### ABSTRACT

We have modeled the peculiar bidimensional shape of the emission lines in a sample of four disk galaxies as due to the motion of a gaseous disk rotating in the combined potential of a central point-like mass and of a diffuse stellar disk. From the values we derive for the central masses and the luminosities of the corresponding bulges we obtain a median  $M_\bullet/L_{B, bulge} \sim 0.16$  (in solar units). This value is one order of magnitude larger than the median value derived by Ho (1998) but still within the scatter.

*Subject headings:* galaxies: kinematics and dynamics — galaxies: nuclei — galaxies: individual (NGC 2179, NGC 4343, NGC 4435, NGC 4459, NGC 5064) — galaxies: structure

---

<sup>1</sup>Based on observations carried out at ESO, La Silla, (Chile) (ESO N. 58, A-0564) and on observations with INT operated on the island La Palma by the Royal Greenwich Observatory in the Spanish Observatorio del Roque de Los Muchachos of the Instituto de Astrofísica de Canarias, Tenerife, Spain.

<sup>2</sup>Dipartimento di Astronomia, Università di Padova, Vicolo dell’Osservatorio 5, I-35122 Padova, Italy

<sup>3</sup>Osservatorio Astrofisico di Asiago, Dipartimento di Astronomia, Università di Padova, Via dell’Osservatorio 8, I-36012 Asiago, Italy

<sup>4</sup>European Southern Observatory, Alonso de Cordova 3107, Casilla 19001, Santiago 10, Chile

<sup>5</sup>Telescopio Nazionale Galileo, Osservatorio Astronomico di Padova, Vicolo dell’Osservatorio 5, I-35122 Padova, Italy

## 1. Introduction

There is an increasing evidence of conspicuous mass concentrations in the center of galaxies, lending support to the idea that their central engine is constituted by a black hole (e.g., see Kormendy & Richstone 1995 and Ho 1998 for a recent review). This evidence comes both from stellar and gaseous dynamics. In this latter case the mass concentration is deduced by the observation of an increasing of the rotation velocity of the gas in a disk towards the center, according to Kepler's third law. Seven of such circumnuclear Keplerian disks (hereafter CNKD) have been up to now discovered: four CNKDs have been observed using the high resolution capability of the *Hubble Space Telescope (HST)* (Ferrarese et al. 1996, Macchetto et al. 1997, Bower et al. 1998, van der Marel & van den Bosch 1998), while three were detected with Very Long Baseline Interferometry (VLBI) and Very Long Baseline Array (VLBA) observations of the maser sources (Miyoshi et al. 1995, Greenhill & Gwinn 1997, Greenhill, Moran & Herrnstein 1997).

In a program aimed to study at high spatial and spectral resolution the structure of the emission lines in the nuclear regions of early-type disk galaxies, we have obtained spectra of the nuclei of eight galaxies with the 3.6-m telescope at La Silla and the 2.5-m Isaac Newton telescope (INT) at La Palma. In almost all cases the structure of the emission lines is complex. In this paper we show that in one galaxy extracted from our sample (NGC 2179) and in three galaxies taken from the sample studied by Rubin et al. (1997) (NGC 4343, NGC 4435 and NGC 4459) it is possible to recognize the kinematic behaviour typical of a CNKD, thus demonstrating the feasibility of their detection with optical ground-based telescopes.

## 2. Observations and data reduction

The spectroscopic observations of the southern hemisphere objects of our sample (the Sa galaxies NGC 2179, NGC 3281, NGC 5064 and the Sb NGC 2815) were carried out at the 3.6-m ESO Telescope in La Silla on February 3-4, 1997. The telescope was equipped with the Cassegrain Echelle Spectrograph (CASPEC) mounting the Long Camera in long-slit configuration without the crossdisperser. The 31.6 lines mm<sup>-1</sup> grating was used in combination with a 1''.3×2''.4 slit. The spectral order #86 ( $\lambda_c = 6617 \text{ \AA}$ ) corresponding to the redshifted H $\alpha$  region was isolated by means of the narrow-band 6630/51 Å filter. It yielded a wavelength coverage of about 21 Å between 6630 Å and 6651 Å with a reciprocal dispersion of 3.17 Å mm<sup>-1</sup>. The adopted detector was the No. 37 1024×1024 TK1024AB CCD with a 24×24  $\mu\text{m}^2$  pixel size. No on-chip binning was done and each pixel corresponds to 0.076 Å×0''.33. The observations of the northern hemisphere sample objects (the S0 NGC 2768, the Sa NGC 3898 and NGC 4698 and the SBab NGC 4419) were obtained at the 2.5-m INT in La Palma on March 19-21, 1996. The spectra were taken with the Intermediate Dispersion Spectrograph (IDS). The H1800V 1800 grooves mm<sup>-1</sup> grating was used in the first order in combination with the a 1''.9×4''.0 slit, the 500 mm camera and the AgRed

collimator. It yielded a wavelength coverage of about 240 Å between 6650 Å and 6890 Å with a reciprocal dispersion of 9.92 Å mm<sup>-1</sup>. As before no on-chip binning was done on the available 1024×1024 TK1024A CCD and each 24×24  $\mu\text{m}^2$  pixel corresponds to 0.24 Å×0''.33.

We took for NGC 2179 and NGC 5064 six and four separate major-axis spectra centered on the nucleus for a total exposure time of 360 and 240 minutes respectively. The galaxies were centered on the slit using the guiding camera at the beginning of each exposure. Comparison thorium-argon lamp exposures were obtained before and after each object integration. The value of the seeing FWHM during the observing nights was between 0''.8 and 1''.2 as measured by the La Silla Differential Image Motion Monitor (DIMM). Using standard MIDAS<sup>6</sup> routines the spectra were bias subtracted, flat-field corrected, cleaned for cosmic rays and wavelength calibrated. Cosmic rays were identified by comparing the counts in each pixel with the local mean and standard deviation, and then corrected by substituting a suitable value. The instrumental resolution was derived by measuring the FWHM of  $\sim 30$  single emission lines distributed all over the spectral range of a calibrated comparison spectrum. It corresponds to a FWHM = 0.233 ± 0.017 Å (i.e.  $\sim 11$  km s<sup>-1</sup> at H $\alpha$ ). The single spectra of the same object were aligned and co-added using their stellar-continuum centers as reference. In each spectrum the center of the galaxy was defined by the center of a Gaussian fit to the radial profile of the stellar continuum. The contribution of the sky was determined from the edges of the resulting frame and then subtracted. To study the H $\alpha$  emission line, we subtracted the underlying stellar continuum which was determined by averaging a 2.5 Å wide region with high S/N adjacent to the H $\alpha$  line. A constant stellar continuum provides a good match to the underlying distribution within this narrow wavelength range and avoids possible spurious effects caused by higher order interpolations. For the purpose of this paper the subtraction of a continuum with the proper H $\alpha$  absorption is not crucial.

### 3. Results

All galaxies of our sample with the exception of NGC 5064 have emission lines (our spectrum covers a range centered on H $\alpha$ ) characterized by the presence of two apparently distinct components. The first component gives rise to an extended rotation curve which flattens at a given distance from the center. The second component has the aspect of a broad line which is very little extended spatially. The FWHM of this line is usually of the same order of magnitude of the observed velocity range  $\Delta v$  of the rotation curve. In the case of NGC 2179 the central component is slightly tilted suggesting rotation [ $v(0''.6) - v(-0''.6) \sim 200$  km s<sup>-1</sup>]. In the remaining cases the broadening of the line can be due either to turbulent motions or to rotation which we are not able to measure due to a lack of spatial resolution.

To the aim of the present study we concentrate our attention on the case of NGC 2179. In

---

<sup>6</sup>MIDAS is developed and maintained by the European Southern Observatory

this object the observed velocity is apparently double valued at the same projected distance from the nucleus giving rise to a very peculiar shape of the emission lines. The emission lines reach a value of  $250 \text{ km s}^{-1}$  at  $R = 1''.5$  and then decrease to  $180 \text{ km s}^{-1}$  at  $R = 3''$ . At this point the velocity turns to increase till it reaches an approximately constant value of  $\sim 200 \text{ km s}^{-1}$  at  $R = 6''$  (See Fig. 1a). The same phenomenon has been observed also by Rubin et al. (1997) in the following early-type disk galaxies: NGC 4343 (Sa), NGC 4435 (S0) and NGC 4459 (S0). One of the other characteristics of the emission lines in the four just mentioned galaxies is the lack of a central intensity peak which, on the contrary, is present in the remaining galaxies of our sample.

The peculiar and complex bidimensional shape and intensity distribution of the emission lines in these galaxies can be interpreted with a simple model of a gaseous disk orbiting in the combined gravitational potential of a central mass concentration superimposed to that due to the stellar component. We assume that the gas resides in an infinitesimally thin disk whose mean motion is characterized by circular orbits in the plane of the galaxy. At each position  $(x, y)$  on the sky the line-of-sight velocity profile is a Gaussian  $\phi$  with mean  $V(x, y) = V_c(R) x \sin i / R$  and dispersion  $\sigma(R)$ , where  $R^2 = x^2 + (y / \cos i)^2$  is the radius in the disk and  $i$  the inclination of the galaxy. The dispersion is given by  $\sigma^2(R) = \sigma_{\text{gas}}^2(R) + \sigma_{\text{instr}}^2$ , where  $\sigma_{\text{gas}}(R)$  is the intrinsic velocity dispersion of the gas and  $\sigma_{\text{instr}}$  is the instrumental dispersion (assuming a Gaussian instrumental broadening function). The gas dispersion is assumed to be isotropic and has been parametrized through  $\sigma_{\text{gas}}(R) = \sigma_0 + \sigma_1 \exp(-R/R_t)$ , where  $R_t$  is the scale length of the turbulence.

The circular velocity  $V_c(R)$  is produced by the combined potential of a possible central black hole with mass  $M_\bullet$  and of the galaxy stellar component. The contribution to the velocity due to the black hole is given by  $V_\bullet(R) = \sqrt{GM_\bullet/R}$ . The contribution  $V_\star(R)$  due to the stars potential has been directly measured on the emission lines of each spectrum at distances where both the seeing effect and the black hole attraction are negligible, and it has been linearly interpolated for smaller  $R$  by imposing that  $V_\star(0) = 0$ . The resulting intrinsic velocity profile of the disk is then computed as  $V_c^2(R) = V_\bullet^2(R) + V_\star^2(R)$ .

The bidimensional model of the spectrum is given by

$$\Phi(v, S) = \int_{S - \frac{\Delta S}{2}}^{S + \frac{\Delta S}{2}} ds \int_{B - \frac{h}{2}}^{B + \frac{h}{2}} db \iint_{-\infty}^{+\infty} ds' db' \phi[v - V(s', b')] I(s', b') P(s' - s, b' - b) \quad (1)$$

where  $(S, B)$  are the coordinate along the slit and perpendicularly to it respectively, while  $h$  is the slit width and  $\Delta s$  is the pixel size of the detector.  $I(s', b')$  is the intrinsic surface brightness distribution of the disk and has been parametrized as  $I(R) = I_0 + I_1 \exp(-R/R_I)$ , where  $I_0$ ,  $I_1$  and  $R_I$  are free parameters.  $P(s' - s, b' - b)$  is the PSF which has been modeled as a Gaussian, owing to the lack of a specific PSF image obtained at the time of the observations. Note that the parametrizations for  $I(R)$  and  $\sigma_{\text{gas}}(R)$  have been chosen because they are able to adequately reproduce our data, but they have no further physical significance.

The line profile  $\Phi(v, S)$ , rebinned on a grid with steps  $\Delta v$  (reciprocal dispersion) and  $\Delta s$ , can be directly compared to the star-light-subtracted bidimensional spectrum obtained on the CCD.

Using the above model we have obtained for NGC 2179 the simulation of the H $\alpha$  emission line of Fig. 1b which is remarkable for its similarity with the observed one (Fig. 1a). Note that our smooth model does not try to reproduce the bright knots present in the observed spectrum. These knots are due to spiral arms which are also visible in our H $\alpha$  imaging. The black hole mass of the best-fit model is given in Table 1. Similar models have been constructed for the three galaxies observed by Rubin et al. (1997) and the best-fit black hole masses are also given in the same table.

#### 4. Discussion

In the previous paragraphs we have shown that the peculiar shape of the emission lines in a sample of four galaxies is consistent with the effect produced by the combined potential of a central point-like mass concentration and of a diffuse stellar component. Previous galaxies modeled with CNKD (for references see the Introduction) were all ellipticals and this latter component does not play a significant role due to the very limited spatial regions sampled. On the contrary our sample is constituted by disk galaxies with extended emission lines, therefore we observe the effect of both components. In this way we were able to point out the presence of central mass concentrations of the order of  $1 \times 10^9 M_\odot$  in a sample of disk galaxies, using ground-based observations by modeling the disturbances produced by these concentrations on the rotation curve of the disk component. We have simulated the shape of the emission line as a function of the central mass: the higher the disturbance, the largest the central mass. In Fig. 1d we show the limiting case of the simulation for the lowest mass detectable with our instrumental setup. Fig. 1c presents the H $\alpha$  region of the spectrum of the galaxy NGC 5064, which does not present any peculiar central structure. We conclude that in this galaxy either the central mass is lower than  $5 \times 10^7 M_\odot$  or the Keplerian part of the gaseous disk we considered in the model is missing.

With the observations presented in this paper we have demonstrated the possibility of detecting central mass concentrations in galaxies with ground-based telescopes properly equipped using the CNKDs as probes. The masses which can be determined are larger than  $5 \times 10^7 M_\odot$  at the distance of the Virgo cluster. Up to now the higher resolution offered by HST has not contributed to the detection of central masses lower than this limit. In fact the four galaxies so far studied with HST posses central masses of the same order of ours. A simulation similar to the one used in this paper predicts that HST, equipped with the Space Telescope Imaging Spectrograph will allow to detect central masses down to the level of  $5 \times 10^6 M_\odot$ . Note that although VLBI spectroscopy of H<sub>2</sub>O masers delivers much higher angular resolution, this technique is limited by the availability of suitably bright sources. We think that this detection of lower mass black holes will constitute one of the most proper use of HST. The additional advantage of HST is that it allows to put stringent constraints in the size of the regions containing the central mass, which is an hopeless task with ground-based observations.

For the four galaxies discussed in this paper we can summarize our measurements with a single median value  $M_\bullet/L_{B, bulge} \sim 0.16$  (in solar units). This value is one order of magnitude

larger than the median value derived by Ho (1998) from a sample of 20 objects but still within the scatter. Assuming an  $M/L \sim 6$  typical of old stellar populations (van der Marel 1991) this ratio translates to a  $M_{\bullet}/M_{bulge} \sim 0.03$ .

We thank Dave Burstein and Vera Rubin for helpful discussions. This research has made use of the NASA/IPAC Extragalactic Database (NED) which is operated by the Jet Propulsion Laboratory, California Institute of Technology, under contract with the National Aeronautics and Space Administration.

Table 1. Parameters of the modeled galaxies.

object [name] (1)	type [RSA] (2)	type [RC3] (3)	$B_T^0$ [mag] (4)	P.A. [ $^\circ$ ] (5)	$i$ [ $^\circ$ ] (6)	$V_\odot$ [km s $^{-1}$ ] (7)	$D$ [Mpc] (8)	scale [pc $''^{-1}$ ] (9)	$M_{B,bulge}$ [mag] (10)	$M_\bullet$ [10 $^8$ M $_\odot$ ] (11)
NGC 2179 <sup>a</sup>	Sa	SAS0	12.83	170	51	2885 $\pm$ 15	35.6	172.6	-19.07	10
NGC 5064 <sup>a</sup>	Sa	PSA2*	11.67	38	65	2980 $\pm$ 15	36.7	177.9	-19.78	< 0.5
NGC 4343 <sup>b</sup>	...	SAT3*	12.37	133	78	1002 $\pm$ 10	17.0	82.4	-17.24	5
NGC 4435 <sup>b</sup>	SB0 <sub>1</sub> (7)	LBS0	11.61	13	90	806 $\pm$ 10	17.0	82.4	-18.93	10
NGC 4459 <sup>b</sup>	S0 <sub>3</sub> (3)	LAR+	11.21	110	42	1183 $\pm$ 10	17.0	82.4	-19.20	10

<sup>a</sup>From our sample

<sup>b</sup>from the sample of Rubin et al. (1997)

Note. — Col.(2): morphological classification from Sandage & Tamman (1981). Col.(3): morphological classification from de Vaucouleurs et al. (1991, hereafter RC3). Col.(4): total  $B$  magnitude after correcting for extinction and redshift from RC3. Col.(5): major-axis position angle from RC3. Col.(6): inclination from Rubin et al. (1997) except for NGC 2179 and NGC 5064 (Tully 1988). Col.(7): heliocentric systemic velocity derived as the center of symmetry of the gas rotation curve. For NGC 2179, NGC 5064 it is taken from our data, and for NGC 4343, NGC 4435, NGC 4459 it is taken from Rubin et al. (1997). Col.(8): distance of NGC 2179 and NGC 5064 is derived from the heliocentric velocity corrected for the motion of the Sun with respect of the Local Group by  $\Delta V = 300 \cos b \sin l$  with  $H_0 = 75$  km s $^{-1}$  Mpc $^{-1}$ . The galaxies of the Rubin's sample are members of the Virgo cluster and we assumed a distance of 17 Mpc (Freedman et al. 1994). Col.(10): statistical estimate of the absolute  $B$  magnitude of the bulge derived following Simien & de Vaucouleurs (1986). Col.(11): value of the central mass concentration derived as described in Sect. 3

## REFERENCES

Bower, G.A., Green, R.F., Danks, A., Gull, T., Heap, S., Hutchings, J., Joseph, C., Kaiser, M.E., Kimble, R., Kraemer, S., Weistrop, D., Woodgate, B., Lindler, D., Hill, R.S., Malumuth, E.M., Baum, S., Sarajedini, V., Heckman, T.M., Wilosn, A.S., & Richstone, D.O. 1998, *ApJ*, 492, L111

de Vaucouleurs, G., de Vaucouleurs, A., Corwin, H.G., Jr., Buta, R.J., Paturel, G., & Fouqué, R. 1991, Third Reference Catalogue of Bright Galaxies (New York: Springer-Verlag) (RC3)

Ferrarese, L., Ford, H.C., & Jaffe, W. 1996, *ApJ*, 470, 444

Freedman, W.L., Madore, B.F., Mould, J.R., Ferrarese, L., Hill, R., Kennicutt, R.C., Jr., Saha, A., Stetson, P.B., Graham, J.A., Ford, H., Hoessel, J.G., Hucra, J., Hughes, S.M., & Illingworth, G.D. 1994, *Nature*, 371, 757

Greenhill, L.J., & Gwinn, C. 1997, *Ap&SS*, 248, 261

Greenhill, L.J., Moran, J.M., & Herrnstein, J.R. 1997, *ApJ*, 481, L23

Ho, L.C. 1998, in Observational Evidence for Black Hole in the Universe, ed. S.K. Chakrabati (Dordrecht: Kluver Academic Publishers), in press [astro-ph/9803307]

Kormendy, J., & Richstone, D. 1995, *ARA&A*, 33, 581

Macchetto, F., Marconi, A., Axon, D.J., Capetti, A., Sparks, W., & Crane, P. 1997, *ApJ*, 489, 579

Miyoshi, M., Moran, J., Herrnstein, J., Greenhill, L.J., Nakai, N., Diamond, P., & Inoue, M. 1995, *Nature* 373, 127

Rubin, V.C., Kenney, J.D.P., & Young, J.S. 1997, *AJ*, 113, 1250

Sandage, A., & Tammann, G.A. 1981, A Revised Shapley-Ames Catalog of Bright Galaxies (Washington: Carnagie Institution)

Simien, F., & de Vaucouleurs, G. 1986, *ApJ*, 302, 564

Tully, R.B. 1988, *Nearby Galaxies Catalog* (Cambridge: Cambridge University Press)

van der Marel, R.P. 1991, *MNRAS*, 253, 710

van der Marel, R.P., & van den Bosch, F.C. 1998, *AJ*, submitted [astro-ph/9804194]

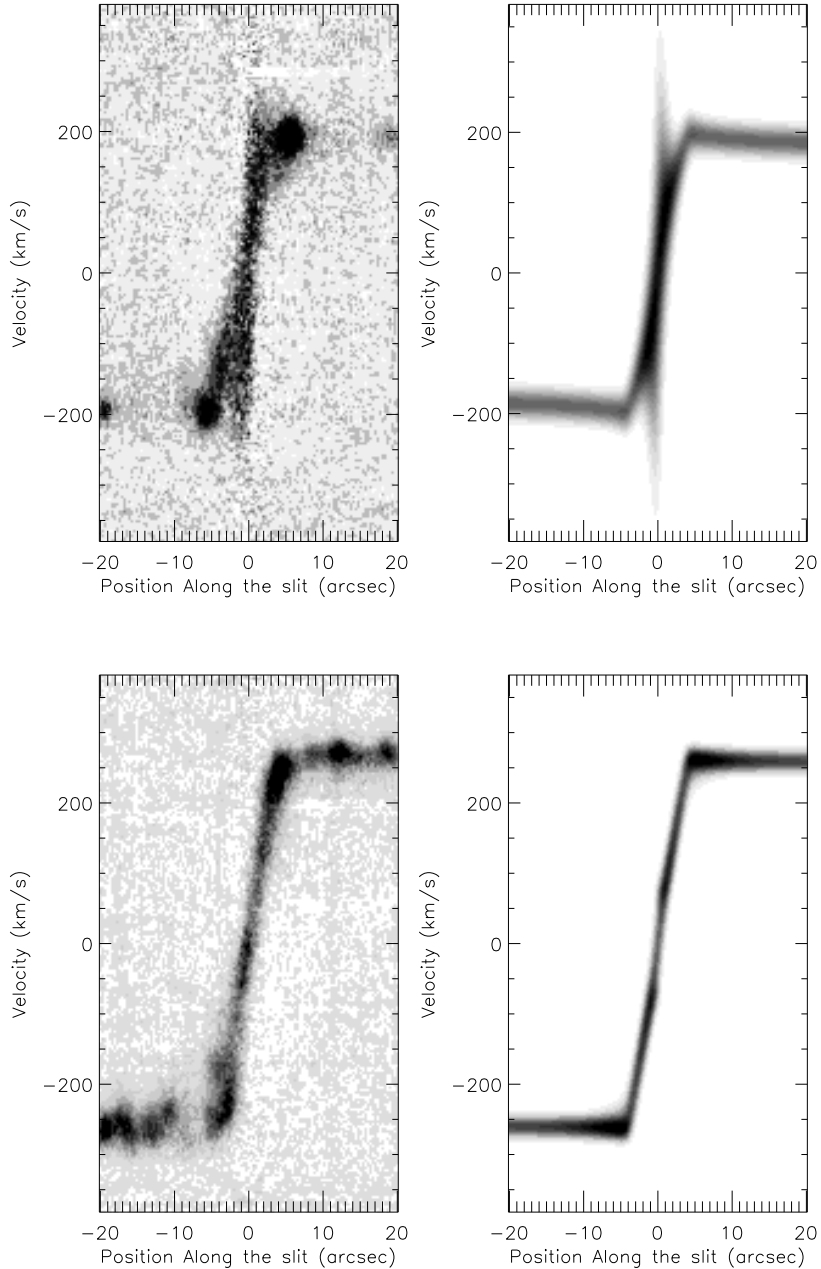


Fig. 1.— *Upper left (a)*: The H $\alpha$  emission line, observed along the major axis of NGC 2179, after subtraction of the stellar continuum. *Upper right (b)*: Our model of the H $\alpha$  emission line of NGC 2179 [on the same scale of (a)]. The best fit is obtained with a central black hole of mass  $M_{\bullet} = 1 \times 10^9 M_{\odot}$ . *Lower left (c)*: Same as (a) for NGC 5064. *Lower right (d)*: Same as (b) for NGC 5064. The highest black hole mass which can be added without significantly disturbing the general shape of the H $\alpha$  line ( $M_{\bullet} = 5 \times 10^7 M_{\odot}$ ) has been adopted in this model.